NRC Research Press

ARTICLE

Further studies of incipient motion and shear stress on local scour around bridge abutment under ice cover

Peng Wu, Faye Hirshfield, and Jueyi Sui

Abstract: An experimental study was conducted to investigate the scour development around bridge abutments under ice cover with non-uniform natural sands. Two abutments and three non-uniform sediments were used in the research. The mechanism of incipient motion for non-uniform sediments under ice cover was analyzed. By introducing scour angles around two abutments, a relationship between maximum scour depth and velocity was established for clear-water scour under ice cover. Dimensionless shear stress was also calculated and compared with shear Reynolds number for non-uniform sediments. The maximum scour depth and dimensionless shear stress were investigated under both open channel, smooth cover and rough covered conditions. Results show that around the square abutment, the scour angle is smaller than that of the semi-circular abutment. For clear water scour, the maximum scour depth increases due to the presence of ice cover.

Key words: bridge abutment, dimensionless shear stress, ice cover, incipient motion, scour angle.

Résumé : Une étude expérimentale a été réalisée pour examiner le développement de l'affouillement autour de butées de pont sous le couvert de glace avec des sables naturels à granulométrie variable. Deux butées et trois sédiments à granulométrie variable ont été utilisés lors de la recherche. Le mécanisme d'initiation du mouvement pour les sédiments à granulométrie variable sous couvert de glace a été analysé. L'introduction d'angles d'affouillement autour des deux butées a permis d'établir une relation entre la profondeur maximale d'affouillement et la vitesse pour l'affouillement en eau claire sous couvert de glace. Une contrainte de cisaillement sans dimension a également été calculée et comparée au nombre de cisaillement de Reynolds pour les sédiments non uniformes. La profondeur maximale d'affouillement et la contrainte de cisaillement sans dimension ont été examinées sous des conditions de canalisation à écoulement libre, avec un revêtement lisse et avec un revêtement rugueux. Les résultats montrent que l'angle d'affouillement autour de la butée carrée est inférieur à celui autour d'une butée semi-circulaire. La profondeur d'affouillement maximale en eau claire augmente en raison de la couverture de glace. [Traduit par le Rédaction]

Mots-clés : butée de pont, contrainte de cisaillement sans dimension, couvert de glace, initiation du mouvement, angle d'affouillement.

Introduction

Local scour refers to the scour caused by river obstructions such as bridge abutments, piers, and other objects that obstruct the flow (Chang 2002). It has been identified as an important issue by civil engineers for a long time. Excessive scour can cause structural failure and even result in the loss of life. According to Melville (1992), 29 of 108 bridge failures in New Zealand between 1960 and 1984 were attributed to abutment scour. Over the past few decades, local scour around bridge abutments has received worldwide attention: Laursen and Toch (1956), Froehlich (1995), Melville (1997), Coleman et al. (2003), and Dey and Barbhuiya (2005). However, almost all of these studies were conducted in open channels.

In the Northern Hemisphere, winter lasts up to six months, which is a big challenge for hydraulic engineers to estimate scour condition around bridges. As mentioned by Ettema et al. (2011), local scour around bridge structures under certain conditions remain insufficiently understood. For example, ice accumulation can further complicate the flow field and the scour under ice cover is still not fully researched. To fill this gap, some researchers started to look at this problem from an experimental approach (Ackermann et al. 2002; Hains 2004; Munteanu 2004; Ettema and Daly 2004; Munteanu and Frenette 2010) and numerical simulation as mentioned by Ettema et al. (2000).

Ackermann et al. (2002) investigated the effects of ice cover on local scour around bridge piers. By using uniform sediments, the authors found that for equivalent averaged flow velocities, the existence of an ice cover could increase the local scour depth by 25%~35%. For live bed scour, a rough cover gave a slightly larger scour depth than smooth cover. Munteanu (2004) conducted experiments on local scour around cylinders and found that under clear water conditions local scour increased up to 55%. Wang et al. (2008) discussed the role of flow velocity and critical shear Reynolds number for incipient motion of bed materials. The effects of grain size on densimetric Froude number for incipient motion were also investigated. As reported in their paper, the mean flow velocity for incipient motion under ice cover decreases with the increase in the roughness of ice cover. As reported by Sui et al. (2010), under ice covered conditions, flow velocity profiles can be divided into the upper portion, which is from the ice cover bottom to the point of the maximum velocity, and the lower portion, which is from the channel bed to the maximum velocity. When the channel bed and ice cover have different resistance coefficients, the maximum velocity will be closer to the surface with the smaller resistance coefficient. Wu et al. (2014) conducted flume experiments to study the maximum scour depth under ice covered conditions around abutments. They found that with the in-

Received 4 December 2013. Accepted 7 September 2014.

P. Wu, F. Hirshfield, and J. Sui. Environmental Engineering, University of Northern British Columbia, Prince George, BC V2N 4Z9, Canada.
Corresponding author: Jueyi Sui (e-mail: Jueyi.Sui@unbc.ca).

Published at www.nrcresearchpress.com/cjce on 9 September 2014.

crease in ice cover roughness, the maximum scour depth also increases correspondingly.

In practice, dimensionless shear stress is used to study the incipient motion. Dey and Barbhuiya (2005) investigated the three dimensional turbulent flow properties around a short vertical wall abutment both upstream and downstream of the scour hole in open channels. By using the Reynolds stresses, the bed shear stresses were also calculated. From their experiments, the maximum bed shear stresses were about 3.2 times that of the incoming flow. Duan et al. (2009) examined the Reynolds stresses around a spur dike. It was found that the Reynolds stress was 2–3 times that of the incoming flow. Since the abutment and spur dike have similar contraction impact on the flow, all three studies showed the similar amplification factor of bed shear stress in open channel flow.

For non-uniform sediments, finer materials can be more mobile than coarser materials under constant flow conditions. The remaining coarser layer is called armor layer (Yang 2003). With the development of an armor layer, further sediment transport is inhibited. Non-uniform sediment makes up typical bed composition in natural rivers.

The forces acting on a sediment particle at the bottom of the scour hole under ice cover are shown in Fig. 1. For most natural rivers, the river slopes are small enough that the component of gravitational force acting on the particle in the direction of flow can be neglected. As shown in Fig. 1, the forces to be considered related to the incipient motion are the drag force F_D, lift force F_L, submerged weight W, and the resistance force F_R. The angle of the scour hole with vertical abutment is α.

A sediment particle is at a state of incipient motion when the following conditions have been satisfied:

$$(1)\qquad \begin{cases} F_D = F_R \sin\alpha \\ W = F_L + F_R \cos\alpha \end{cases}$$

To date, there are no known experimental studies on clear water scour around bridge abutments under ice covered conditions with non-uniform sediments. The effects of ice cover and armor layer have to be considered in the analysis of local scour. In this study, eq. (1) is used as the frame for further analysis of incipient motion under ice cover. A particle force analysis under ice cover is conducted by introducing armor layer particle size. Then the dimensionless shear stress is calculated.

Experimental setup and measurement

Experiments were conducted in a 40 m long, 2 m wide, and 1.3 m deep flume located at Quesnel River Research Center, BC, Canada (Fig. 2*a*). The flume had a bottom slope of 0.2% and a 90 m^3 volume holding tank was located in the upstream section of the flume to keep a constant flow rate in the experimental zone. At the end of the holding tank, water overflowed from a rectangular weir to flow dissipaters in the experimental zone. Two types of ice cover were used in the research, namely smooth cover and rough cover. The ice cover was 7 m long, which covered the experimental sand box area completely. Two abutment models were made from plexi-glass, semi-circular and square abutments (Fig. 2*b*). The abutment model was located in the middle of the sand box to simulate a bridge abutment with a solid foundation in the river bed. A smooth ice cover was created from Styrofoam panels, while a rough ice cover was created by attaching small cubes of the Styrofoam to the underside of the smooth ice cover. The small cubes had dimensions of 2.5 cm × 2.5 cm × 2.5 cm, with a spacing distance of 3.5 cm from each other. In this study, three different natural non-uniform sediments were used in the flume. The D_{50} of the three sediments was 0.58 mm, 0.50 mm, and 0.47 mm with geometric standard deviations (σ_g) larger than 1.4. The D_{90} of the three sediments was 2.57 mm, 2.09 mm, and 1.19 mm correspondingly.

Fig. 1. Incipient motion in the scour hole under ice cover.

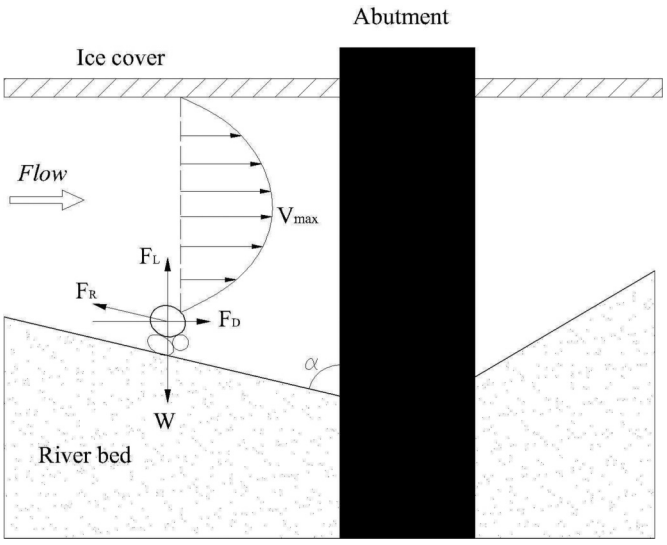

To maintain clear water scour conditions, the approaching velocity was carefully chosen in this series of experiments. A SonTek IQ was installed for flow velocity and water depth measurement. We also used a 10 MHz SonTek down looking ADV for scour hole velocity measurements. The sampling rate of the ADV was 10 Hz. The ADV measurements were mainly located at four points around the square abutment, A, B, C, and D. Around the semi-circular abutment, the measurement points (from A to K) were along measuring lines marked on the abutment (Fig. 2*b*). In the following passage, upstream refers to the section before the abutment in the sand box while downstream refers to the section after the abutment in the flow direction.

For the ADV measurement, two values were used to ensure the measurements can provide an accurate representation of the flow velocity: signal-to-noise ratio (SNR) larger than 15 db and the correlation (COR) between 70% and 100%. Then the data was analyzed by WinADV (Wahl 2000). Figure 3 shows one measurement of the flow field under smooth cover in the scour hole. It can be noted that there is a difference in the velocity field between the scour hole and above the original bed. However, due to the limitations of the ADV, the velocity profile close to the ice cover cannot be completely measured. A decreasing tendency can still be noted because of ice cover presence.

The presence of ice cover in natural rivers can result in an increase in water depth up to about 10%. By using a Styrofoam form in the present research, the cover has very limited impacts on the water depth because of the light weight of the cover. As all experiments were controlled experiments, the flow rate and flow depth had to be constant when other variables were changed. So it should be noted that with the presence of ice cover, flow rate and water depth were maintained constant. Additionally, smooth ice cover here refers to the ice conditions in early winter, while the rough cover refers to the conditions in early spring with ice jam. To reduce the uncertainties of the research, several tests were conducted before the experimental study. Results showed consistency, indicating that the flume was well prepared for the research.

Results and discussion

Incipient motion under ice cover

Equation (1) is used as the frame of force analysis for a sediment particle. By using the criteria from Yang (2003) for incipient motion, the drag force can be expressed as

Fig. 2. Sketch of (a) experimental setup and (b) abutment dimension.

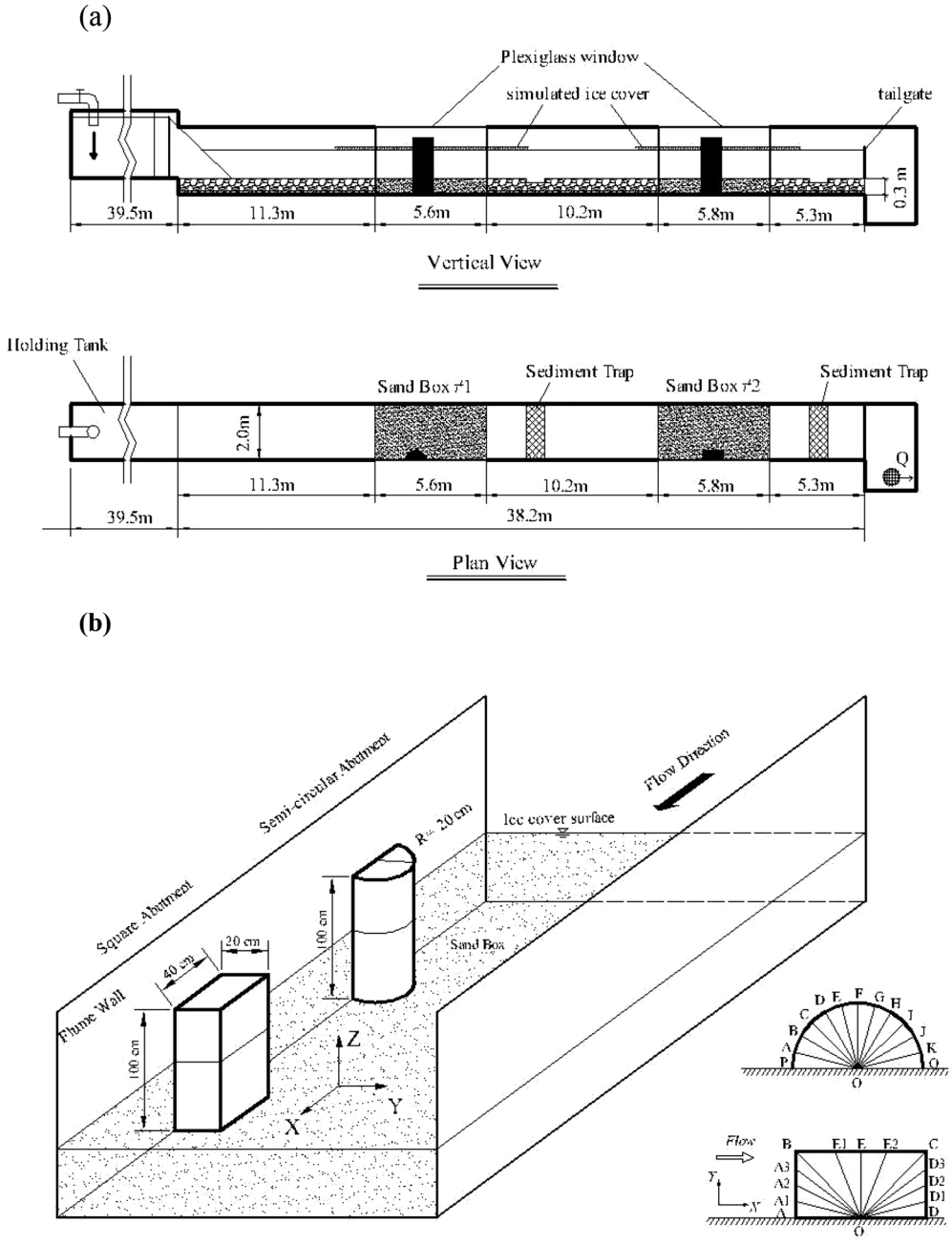

(2) $$F_D = C_D\left(\frac{\pi d^2}{4}\right)\frac{\rho}{2}V_d^2$$

where C_D is the drag coefficient at velocity V_d, ρ is the density of water, and V_d is the local velocity at a distance d above the bed; in this case, d refers to the diameter of the sediment particle. In open channels, the shear velocity, shear stress or flow velocity profile can be calculated by using the logarithmic distribution law. The lift force acting on the particle can be obtained as

(3) $$F_L = C_L\left(\frac{\pi d^2}{4}\right)\frac{\rho}{2}V_d^2$$

where C_L is the lift coefficient at velocity V_d.

The submerged weight of the particle can be given by

(4) $$W = \frac{\pi d^3}{6}(\rho_s - \rho)g$$

By substituting eqs. (2–4) to eq. (1), the following relationship can be found:

(5) $$V_d = \sqrt{\frac{4}{3}\left(\frac{\Delta\rho}{\rho}\right)gd\left(\frac{1}{C_D ctg\alpha + C_L}\right)}$$

The lift coefficient and drag coefficient can be determined by experiments. Since the sediments used here are non-uniform sed-

Fig. 3. Three dimensional velocity profile under smooth ice cover condition (D_{50} = 0.47 mm).

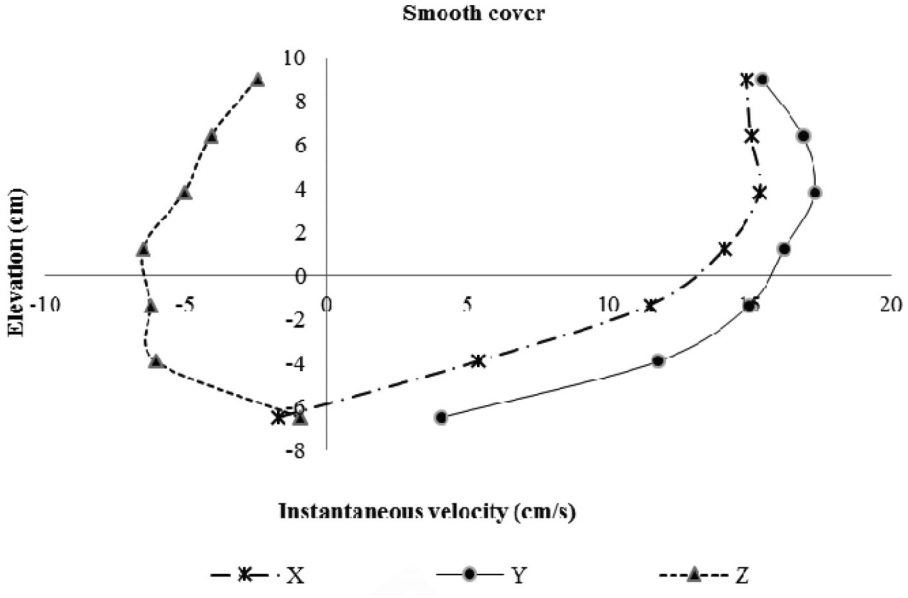

iment, in eq. (5), the diameter of the sediment particle will be replaced by D_{50}, and the following can be derived:

$$V_d = \sqrt{\frac{4}{3}\left(\frac{\Delta\rho g}{\rho}\right)\left(\frac{1}{C_D ctg\alpha + C_L}\right)D_{50}} \quad (6)$$

Regarding the drag coefficient C_D, since the Reynolds number in this research was larger than 10^5, the Stokes Law cannot be applied. By referring the relationship between drag coefficient and Reynolds number for a sphere, developed by Graf and Acaroglu (1966), the value of C_D can be determined. For the lift coefficient C_L, the lift coefficient was a function of shape and density of the sediment particle. With the increase in particle size, C_L should also be increased. In the present study, two Reynolds numbers can be generated. By referring to Fig. 1.2 from Yang (2003), C_D = 0.5 is used for calculation. When a particle is ready to move on the bottom of the open channel, by referring to eq. 2.23 (Yang 2003), C_L is experimentally calculated by considering median sizes of the particle.

From eq. (6), one can note that, with the increase in scour angle, the velocity needed to move the particle in the scour hole will increase correspondingly. When the scour angle is equal to 90°, the velocity reaches maximum. However, when the scour angle is less than 90° the critical velocity for incipient motion in the scour hole will be smaller compared to that with flat beds under the same flow conditions.

Because most of the present equations to calculate velocity are under open channel conditions, it is necessary to note that there are limitations of eq. (6) to be used for the calculation of velocity in the scour region. In the present study, eq. (6) is used as a conceptual approach to study the incipient motion under ice cover.

It is important to note that due to the shortage of flow measurement in the scour hole, there are no available mathematical expressions that can be used to calculate incipient velocity in the scour region. Hence, in the present research, the above equations have limitations for the calculation of incipient motion under ice cover in the scour hole.

Around the square abutment, the maximum scour depth was located around point B, herein, the measurements at B were used to calculate the near bed velocity. While for the semi-circular abutment, the maximum scour depth was located between point D and E, so the measurements at these two points were used.

Under ice cover, if the flow velocity profile was available, as suggested by Kuhnle et al. (2008), the bed shear velocity can be calculated by fitting a least square regression to flow velocity and distance measurements from near the bed to 20% of the depth using the following relationship:

$$U_c = \frac{du}{5.75d\lg h} \quad (7)$$

in which, U_c is the critical bed shear velocity, u is the mean flow velocity at a distance of h, which represents the distance from the bed. However, if the velocity profile was not available, the logarithmic velocity distribution assumption was one of the generally accepted methods for calculating the shear velocity based on Prandtl and Einstein correction factor (Einstein 1950).

$$U_c = \frac{u}{5.75\log_{10}\left(\frac{12.27\chi R_h}{D_{50}}\right)} \quad (8)$$

where R_h is the channel hydraulic radius; u is the average cross-sectional velocity; D_{50} is used to represent the particle size since the sediment used in this research is non-uniform sediment; χ is the Einstein multiplication factor, here we used χ = 1; and the ice cover can be included in the channel hydraulic radius. The critical shear velocities were calculated based on eq. (8).

At the end of each experiment, an armor layer developed around the bridge abutment. To assess the impacts of armor layers, Meyer-Peter and Mueller (1948) developed the following equation by using one mean grain size of the bed to calculate the sediment size in the armor layer.

$$D_{arm} = \frac{SH}{K_1\left(n/D_{90}^{1/6}\right)^{3/2}} \quad (9)$$

where D_{arm} is the sediment size in the armor layer; S is the channel slope; H is the mean flow depth; K_1 is the constant number equal to 0.058 when H is in metres; n is the channel bottom roughness or Manning's roughness, and D_{90} is the bed material size where 90% of the material is finer.

Fig. 4. Incipient motion of different sediments with the maximum scour depth.

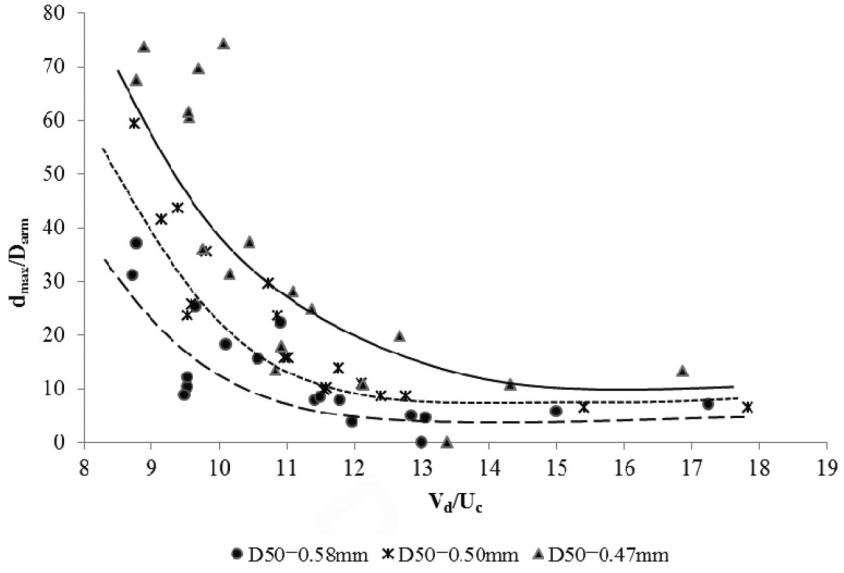

The presence of ice cover in the channel altered the flow characteristics to a great extent. From our observation, the incipient motion started from the toe area of the abutment. Around the square abutment, the scour started at point B and extends to A and E. While around the semi-circular abutment, the scour was firstly observed between point D and E.

The scour angle was calculated by measuring the upstream facing scour distance and maximum scour depth. For the square abutment, the distance from point B to upstream was measured, while for the semi-circular abutment, since the maximum scour depth was located between point D and E, the larger distance outwards from D and E was used. We found that around the square abutment, the average scour angle was 65°, while the average scour angle around the semi-circular abutment was 74°. From the perspective of preventing local scour, the larger the scour angle, the better. Our study indicates the idea that streamline-like abutments cause less local scour depth under ice-covered conditions.

To further examine the relationship between near bed velocity and maximum scour depth, Fig. 4 was plotted. From Fig. 4, at least three observations can be noticed.

1. For the same sediment, with the increase in dimensionless V_d/U_c, the value of d_{max}/D_{arm} decreases correspondingly. From Fig. 4, the velocity impacts on the dimensionless scour depth can be noted. At the beginning, the scour depth increased quickly which means that the scour hole develops fast. Afterward, with the development of the scour hole and formation of the armor layer, the dimensionless scour depth decreased correspondingly. The trend becomes a straight line at the end, which means no variation in scour depth. In other words, the equilibrium scour depth was reached.
2. Under the same flow condition with the same value of V_d/U_c, sediment with smaller D_{50} had a larger maximum scour depth. In this case, sediment with D_{50} = 0.47 mm yielded the largest maximum scour depth compared to other sediments.
3. When the value of V_d/U_c reached approximately 14, the values of d_{max}/D_{arm} had very limited variation, which can tell us that in the scour hole development process, with the formation of the armor layer, the dimensionless scour depth reaches the equilibrium state. In this case, when the particle velocity in the scour hole reaches 14 times of the critical velocity of the sediment, the maximum scour depth is reached.

Dimensionless shear stress

In practice, the shear Reynolds number is usually used to study the incipient motion, which can be given by

$$Re^* = \frac{U_c D}{\nu} \quad (10)$$

in which, U_c is the shear velocity calculated by eq. (8), D is the grain size diameter, and ν is the kinetic viscosity of the fluid. Since the sediment used here is non-uniform sediment, the grain size diameter will be replaced by D_{90}, then eq. (10) can also be written as follows,

$$Re^* = \frac{U_c D_{90}}{\nu} \quad (11)$$

The dimensionless shear stress τ^* is calculated by using the following equation:

$$\tau^* = \frac{\rho U_c^{*2}}{g\Delta\rho D_{90}} \quad (12)$$

where $\Delta\rho$ is the difference in mass density between water and sediment.

The relation between shear Reynolds number and dimensionless shear stress is known as the Shields Diagram, which is widely used for predicting incipient motion in open channels. The calculated criteria for incipient motion of bed material is presented in Fig. 5. For all three non-uniform sediments, with the increase in shear Reynolds number, the dimensionless shear stress increased correspondingly. However, with the same shear Reynolds number, finer sediment had a higher dimensionless shear stress. In this case, sediment with a D_{50} = 0.47 mm had the largest dimensionless shear stress. With a high proportion of finer particles in the non-uniform sediment, the local scour can easily be triggered around bridge abutments. With the same bed material, the larger the shear Reynolds number, the larger the dimensionless shear stress. For the same dimensionless shear stress, the coarser the bed material, the larger the shear Reynolds number.

Fig. 5. The variation of shear Reynolds number with dimensionless shear stress.

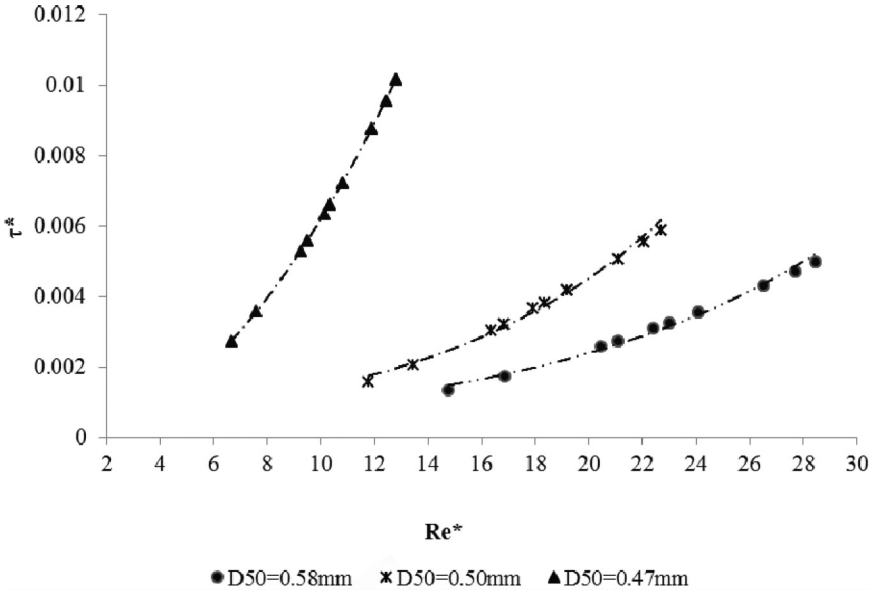

Fig. 6. The maximum scour depth variation with dimensionless shear stress around square and semi-circular abutment.

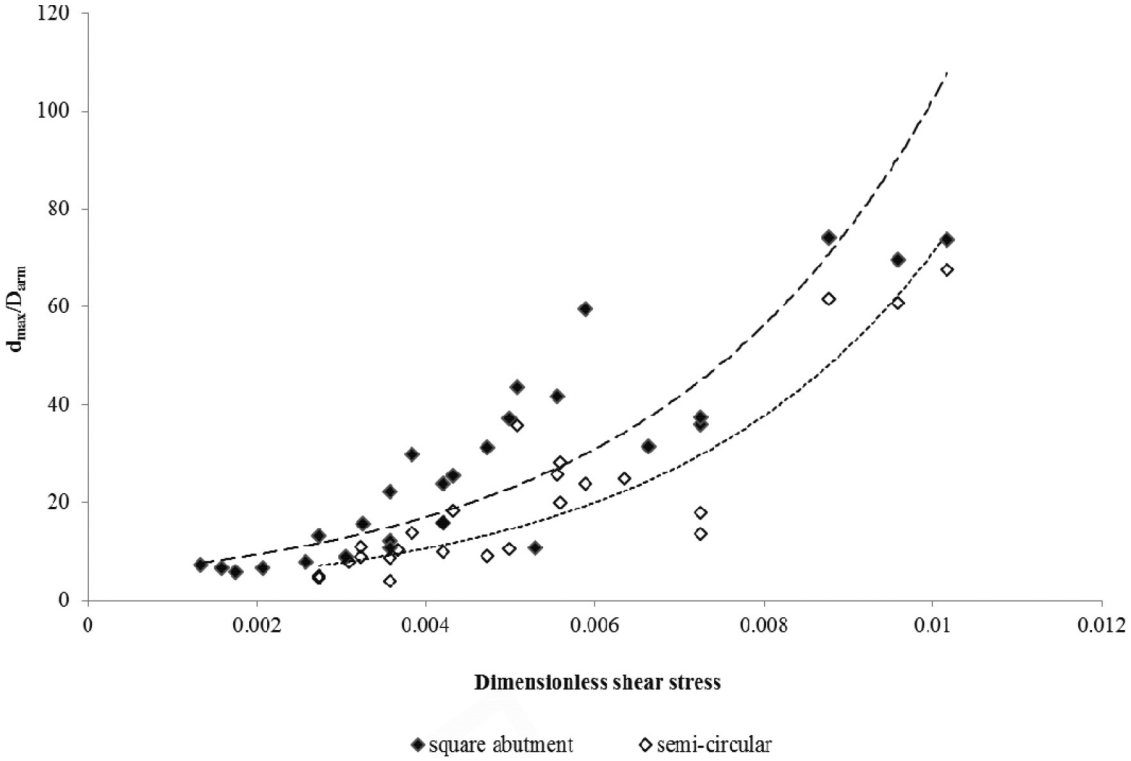

Since the maximum scour depth was our main interest in the scour estimation, the maximum scour depth versus dimensionless shear stress was presented in Figs. 6, 7, and 8. The incipient motion for non-uniform sediment varied more in comparison to that of uniform sediment. To consider the impacts of armor layer in the maximum scour depth, the ratio of maximum scour depth to the particle size of armor layer was developed.

Figure 6 shows the variation of maximum scour depth with the dimensionless shear stress around square and semi-circular abutments under both open channel and ice covered conditions. The overall trend of the curve is increasing. With the increase in dimensionless shear stress, the maximum scour depth increases correspondingly. It is also indicated in the figure that the trend for open channel and covered conditions were the same for different non-uniform sediments. Due to the protection from the armor layer, after the dimensionless shear stress reaches the threshold value, the ratio of maximum scour depth to the particle size of armor layer would be close to constant. However, the experimental data in the present research was not enough to show the overall trend. More data are needed to prove this statement in the future, which means larger dimensionless shear stress will be needed for both open channel and ice covered flow. Furthermore, it can still be noticed that the square abutment has a relatively

Fig. 7. The maximum scour depth variation with dimensionless shear stress under ice cover and open channel (square abutment).

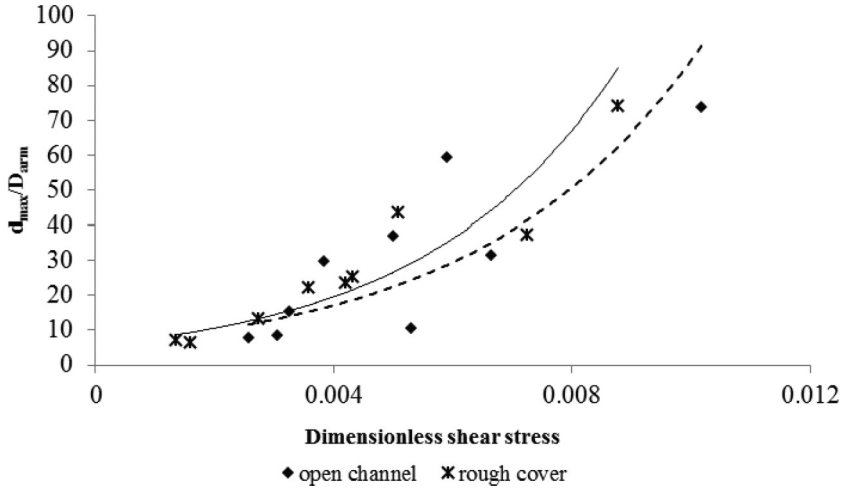

Fig. 8. The maximum scour depth variation with dimensionless shear stress under smooth ice cover and rough ice cover (semi-circular abutment).

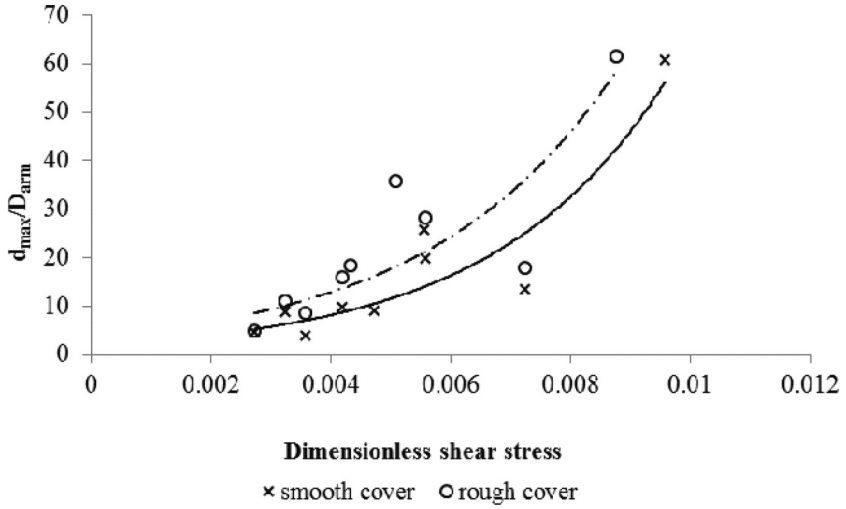

larger dimensionless scour depth compared to that around the semi-circular abutment.

Figure 7 compares the dimensionless shear stress under open channel condition with that of under rough ice covered condition around a square abutment. Figure 8 compared the dimensionless shear stress under smooth ice cover condition with that of under rough covered condition around a semi-circular abutment. For both types of abutments, the maximum scour depth increases with the increase in dimensionless shear stress. Under rough cover, less dimensionless shear stress is needed to reach the same scour depth compared to that for open channel and smooth covered conditions. With the same dimensionless shear stress, rough ice cover results in a deeper scour depth around the abutment compared to that of open flow conditions. Additionally, one can note that rough ice cover can cause a deeper scour depth compared to that under smooth ice covered condition.

Conclusions

The present study investigated the features of incipient motion under ice cover with non-uniform sediments. Experiments have been conducted by using two abutment models and three non-uniform sediments, under open flow condition and two ice-covered conditions. The following are the main conclusions that can be drawn from this study:

1. The average scour angle around a semi-circular abutment is approximately 10° larger than that around the square abutment under clear water conditions. The streamline-like abutment with a solid foundation in the river bed causes less local scour depth than that caused by the square abutment under ice-covered conditions.
2. Based on the scour angle around the bridge abutment, it was found that for the same non-uniform sediment, due to the formation of an armor layer, the maximum scour depth remains constant after the scour hole was formed.
3. With the increase in dimensionless shear stress, the maximum scour depth increases correspondingly. Additionally, the presence of ice cover can result in a deeper maximum scour depth compared to that under open flow condition. In reality, when the ice cover forms in early winter and breaks up in early spring, the roughness coefficient of ice cover (or ice jam) is surprisingly larger than the stable covered period during winter. Therefore the scour depth around the bridge abutment at this time may increase due to the enlarged roughness coefficient.

The present research deals with the incipient motion and dimensionless shear stress for non-uniform sediments under ice-covered conditions. Additionally, due to the shortage of flow

measurements in the scour hole, some empirical equations cited in the paper are under open channel flow conditions. The limitation needs to be considered for further analysis. Further work should include investigation of the flow field in the scour region under ice-covered conditions.

Acknowledgements

Support was given by the Natural Sciences and Engineering Research Council of Canada and UNBC Graduate Research Award (2011–2013). The experiments of this study were conducted at the Quesnel River Research Center (QRRC), BC, Canada. This work represents number 15 in the QRRC publication series. We gratefully acknowledge the help provided by the staff and students Anja Orster, Alex Koiter, Ben Anderson.

References

Ackermann, N.L., Shen, H.T., Olsson, P, and Squire, V.A. 2002. Local scour around circular piers under ice covers. *In* Ice in the environment: Proceedings of the 16th International Symposium on Ice, IAHR, Dunedin, New Zealand, 2–6 December 2002. pp. 149–155.

Chang, H.H. 2002. Fluvial processes in river engineering. 1988. John Wiley & Sons, New York, NY.

Coleman, S.E., Lauchlan, C.S., and Melville, B.W. 2003. Clear-water scour development at bridge abutments. Journal of Hydraulic Research, **41**(5): 521–531. doi:10.1080/00221680309499997.

Dey, S., and Barbhuiya, A.K. 2005. Turbulent flow field in a scour hole at a semicircular abutment. Canadian Journal of Civil Engineering, **32**: 213–232. doi:10.1139/l04-082.

Duan, J.G., He, L., Fu, X., and Wang, Q. 2009. Mean flow and turbulence around experimental spur dike. Advances in Water Resources, **32**: 1717–1725. doi:10.1016/j.advwatres.2009.09.004.

Einstein, H.A. 1950. The bed-load function for sediment transportation in open channel flows. US Department of Agriculture, Soil Conservation Service, Technical Bulletin No. 1026.

Ettema, R., and Daly, S. 2004. Sediment transport under ice. ERDC/CRREL TR-04-20. Cold regions research and Engineering Laboratory, US Army Corps of Engineers. Hanover, NH.

Ettema, R., Braileanu, F., and Muste, M. 2000. Method for estimating sediment transport in ice covered channels. Journal of Cold Regions Engineering, **14**(3): 130–144. doi:10.1061/(ASCE)0887-381X(2000)14:3(130).

Ettema, R., Constantinescu, G., and Melville, B. 2011. Evaluation of bridge scour research: Pier scour processes and predictions. NCHRP Web-only document 175. Transportation Research Board of the National Academies.

Froehlich, D.C. 1995. Armor-limited clear water construction scour at bridge. Journal of Hydraulic Engineering, **121**: 490–493. doi:10.1061/(ASCE)0733-9429(1995)121:6(490).

Graf, W.H., and Acaroglu, E.R. 1966. Settling velocities of natural grains. International Association of Scientific Hydrology, Bulletin **11**(4): 27–43. doi:10.1080/02626666609493492.

Hains, D.B. 2004. An experimental study of ice effects on scour at bridge piers. Ph.D. Dissertation, Lehigh University, Bethlehem, PA.

Kuhnle, R.A., Jia, Y, and Alonso, C.V. 2008. Measured and simulated flow near a submerged spur dike. Journal of Hydraulic Engineering, **134**(7): 916–924. doi:10.1061/(ASCE)0733-9429(2008)134:7(916).

Laursen, E.M., and Toch, A. 1956. Scour around bridge piers and abutments. Iowa Highway Research Board Bulletin, No. 4.

Melville, B.W. 1992. Local scour at bridge abutments. Journal of Hydraulic Engineering, **118**(4): 615–631. doi:10.1061/(ASCE)0733-9429(1992)118:4(615).

Melville, B.W. 1997. Pier and Abutment scour: integrated approach. Journal of Hydraulic Engineering, **123**(2): 125–136. doi:10.1061/(ASCE)0733-9429(1997)123:2(125).

Meyer-Peter, E., and Muller, R. 1948. Formulas for bed-load transport. International Association for Hydraulic Structure, Second meeting, Stockholm, June 1948.

Munteanu, A. 2004. Scouring around a cylindrical bridge pier under partially ice-covered flow condition. Master thesis, University of Ottawa, Ottawa, Ont., Canada.

Munteanu, A., and Frenette, R. 2010. Scouring around a cylindrical bridge pier under ice covered flow condition-experimental analysis. R.V. Anderson Associates Limited and Oxand report.

Smith, B.T., and Ettema, R. 1997. Flow resistance in ice covered alluvial channels. Journal of Hydraulic Engineering, **123**(7): 592–599. doi:10.1061/(ASCE)0733-9429(1997)123:7(592).

Sui, J., Wang, J., He, Y., and Krol, F. 2010. Velocity profiles and incipient motion of frazil particles under ice cover. International Journal of Sediment Research, **25**(1): 39–51. doi:10.1016/S1001-6279(10)60026-1.

Wahl, T.L. 2000. Analyzing data using WinADV. *In* Building Partnerships: Proceedings of the 2000 Joint Conference on Water Resources Engineering and Water Resources Planning and Management. Minneapolis, MN, 30 July–2 August 2000. pp. 1–10. doi:10.1061/40517(2000)300.

Wang, J., Sui, J., and Karney, B.W. 2008. Incipient motion of non-cohesive sediment under ice cover – an experimental study. Journal of Hydrodynamics, **20**(1): 177–124. doi:10.1016/S1001-6058(08)60036-0.

Wu, P., Hirshfield, F., and Sui, J. 2014. Armour layer analysis of local scour around bridge abutments under ice cover. River Research and Applications. doi:10.1002/rra.2771.

Yang, C.T. 2003. Sediment transport, theory and practice. Krieger publishing, Malabar, FL. 412 p.

List of symbols

C_D	drag coefficient at velocity V_d
C_L	lift coefficient at velocity V_d
d_{max}	maximum scour depth around abutments (cm)
D_{50}	mean diameter of sediment for which 50% of the sample is finner (mm)
D_{90}	mean diameter of sediment for which 90% of the sample is finner (mm)
D_{arm}	sediment particle size of armour layer (mm)
F_D	drag force for incipient motion
F_L	lift force
F_R	resistance force
g	gravity acceleration (ms^{-2})
H	mean flow depth
n	Manning's roughness value
Re^*	Reynolds number (-)
S	channel slope
U_c	critical bed shear velocity
u	mean velocity at distance h from the bottom
V_d	incipient motion velocity in the scour hole
W	particle submerged weight
α	scour angle (-)
ρ	density of water
ρ_s	density of sediment
σ_g	geometric standard deviation (-)
τ^*	dimensionless shear stress (-)